materials

MDPI

Article

Alendronate as Bioactive Coating on Titanium Surfaces: An Investigation of CaP–Alendronate Interactions

Ines Despotović [1,*], Željka Petrović [2,*], Jozefina Katić [3] and Dajana Mikić [3]

[1] Division of Physical Chemistry, Ruđer Bošković Institute, Bijenička Cesta 54, 10002 Zagreb, Croatia
[2] Division of Materials Chemistry, Ruđer Bošković Institute, Bijenička Cesta 54, 10002 Zagreb, Croatia
[3] Department of Electrochemistry, Faculty of Chemical Engineering and Technology, University of Zagreb, Marulićev Trg 19, 10000 Zagreb, Croatia; jkatic@fkit.unizg.hr (J.K.); dmikic@fkit.unizg.hr (D.M.)
* Correspondence: ines.despotovic@irb.hr (I.D.); zeljka.petrovic@irb.hr (Ž.P.)

Abstract: The surface modification of dental implants plays an important role in establishing a successful interaction of the implant with the surrounding tissue, as the bioactivity and osseointegration properties are strongly dependent on the physicochemical properties of the implant surface. A surface coating with bioactive molecules that stimulate the formation of a mineral calcium phosphate (CaP) layer has a positive effect on the bone bonding process, as biomineralization is crucial for improving the osseointegration process and rapid bone ingrowth. In this work, the spontaneous deposition of calcium phosphate on the titanium surface covered with chemically stable and covalently bound alendronate molecules was investigated using an integrated experimental and theoretical approach. The initial nucleation of CaP was investigated using quantum chemical calculations at the density functional theory (DFT) level. Negative Gibbs free energies show a spontaneous nucleation of CaP on the biomolecule-covered titanium oxide surface. The deposition of calcium and phosphate ions on the alendronate-modified titanium oxide surface is governed by Ca^{2+}–phosphonate (-PO_3H) interactions and supported by hydrogen bonding between the phosphate group of CaP and the amino group of the alendronate molecule. The morphological and structural properties of CaP deposit were investigated using scanning electron microscopy, energy dispersive X-ray spectroscopy, X-ray diffraction and attenuated total reflectance Fourier transform infrared spectroscopy. This integrated experimental–theoretical study highlights the spontaneous formation of CaP on the alendronate-coated titanium surface, confirming the bioactivity ability of the alendronate coating. The results provide valuable guidance for the promising forthcoming advancements in the development of biomaterials and surface modification of dental implants.

Keywords: titanium dental implant; alendronate coating; calcium phosphate CaP; bioactivity; DFT quantum chemical calculations

Citation: Despotović, I.; Petrović, Ž.; Katić, J.; Mikić, D. Alendronate as Bioactive Coating on Titanium Surfaces: An Investigation of CaP–Alendronate Interactions. *Materials* **2024**, *17*, 2703. https://doi.org/10.3390/ma17112703

Academic Editors: Evgeny Levashov and Csaba Balázsi

Received: 9 April 2024
Revised: 6 May 2024
Accepted: 30 May 2024
Published: 3 June 2024

1. Introduction

Titanium-based materials are the most commonly used for the manufacture of medical implants [1–5], mainly due to their suitable mechanical properties [6]. In addition, titanium and most of its alloys have shown excellent tissue compatibility [7]. However, these materials have been shown to be highly bioinert due to poor contact with the living body upon implantation [8,9]. Since the effectiveness of the osseointegration process with the surrounding tissue depends on the interactions that occur at the outermost surface layer with few atomic distances, the titanium surface has been specifically modified to improve integration with the surrounding tissue and minimize the risks associated with the release of metal ions into the body. Among a number of established approaches to surface modification (functionalization) [10], the formation of a biocompatible and bioactive layer that irreversibly adheres to the surface has attracted particular attention [11–14].

Organophosphorus compounds such as phosphonates have proven to be effective agents for the functionalization of titanium surfaces by forming homogeneous self-assembled monolayers. In particular, alendronate, a nitrogen-containing bisphosphonate, exhibits good coating properties on titanium surfaces [15–17], and the effect of immobilizing alendronate on the titanium surface to stimulate new bone formation and improve bone-implant integration after implantation has been widely reported [17–20]. On the titanium surface, alendronate molecules are covalently bound to the TiO_2 layer via phosphonate groups (-PO_3H) [15]. At the same time, those unbound phosphonate groups (-PO_3H), together with the amine groups (-NH_2) and hydroxyl groups (-OH) of the alendronate molecules, remain free and can participate in the chemical reactions during new bone growth. These reactions include the spontaneous precipitation of different calcium phosphate phases (CaP), including hydroxyapatite (HAp), a naturally occurring form of calcium phosphate that is an essential component for the formation of new bone matrix. The CaP deposit has an important role in initial cell attachment since it can adsorb proteins from the surrounding tissue, promoting cell adhesion and the recruitment of osteogenic cells to the implant surface and facilitating the new bone mineralization process [21–24]. As known from the literature, the chemical precipitation and nucleation of calcium phosphate (CaP) are strongly influenced by self-assembled monolayers carrying different functional groups [25–28]. Specifically, different monolayers with phosphonate (-PO_3H), amino (-NH_2) or hydroxyl (-OH) groups were investigated [29–35], and they were found to promote the mineralization process and affect the texture of the CaP deposit. These results sparked our interest in investigating the potential of alendronate coating as a promoter of CaP formation in the contents of the enhanced bioactivity of the underlying titanium.

In our previous publications, the mechanism of the formation of the alendronate coating on the titanium surface and its chemical stability when exposed to artificial saliva was reported in detail [15,16]. Since the alendronate-modified titanium surface has been shown to exhibit good chemical stability, which is the basic prerequisite for its biocompatibility, it was of great importance to investigate bioactivity as an essential property for successful osseointegration. In this study, the bioactivity potential of the alendronate coating was monitored via the spontaneous formation of CaP deposits on the alendronate-coated titanium surface. To the best of our knowledge, a combined experimental and theoretical approach was used for the first time to fully elucidate the formation of CaP. Quantum chemical DFT calculations provided insights into the interactions of the calcium and phosphate ions with alendronate molecules on the titanium surface in the early phase of the CaP nucleation process. The results indicated spontaneous CaP formation, which was confirmed experimentally using scanning electron microscopy (SEM), energy dispersive X-ray spectroscopy (EDS), X-ray diffraction (XRD) and attenuated total reflection Fourier transform infrared spectroscopy (ATR-FTIR). The phase analysis of the CaP deposit confirmed the mixture of the phases, beta-tricalcium phosphate (β-TCP) and calcium-deficient HAp, having beneficial properties from an application point of view.

2. Materials and Methods

2.1. Quantum Chemical Calculations

Density functional theory (DFT) quantum chemical calculations have been carried out, employing the M06 functional developed by Truhlar's group [36–38]. The 6-31+G(d,p) + LANL2DZ basis set was utilized for geometry optimization. Pople's 6-31+G(d,p) double-ξ, basis set was chosen for the H, C, O, N, Ca, and P atoms, and the LANL2DZ basis set was chosen for the transition metal (Ti) atoms [39]. The vibrational frequency analysis under the harmonic oscillator approximation was used to verify all calculated structures to be true minima on the potential energy surface. In addition, the thermal correction to the Gibbs free energy was derived from the same vibrational analysis. To refine the energy, a highly flexible 6-311++G(2df,2pd) basis set was utilized for H, C, O, N, Ca and P atoms, while the same LANL2DZ ECP-type basis set was used for the titanium atoms. The polarizable continuum solvation model SMD (solvation model based on density) [40] was

used to model the solvation effects. The solvent water is represented by a dielectric constant of ε = 78.3553. To account for the specific interaction of the metal cation with the water solvent, the first solvation shell [41], represented by a specific number of water molecules coordinating the calcium ion, is explicitly included in the quantum chemical region, and the remaining bulk solvent is approximated by a polarizable continuum, leading to the cluster continuum method [42]. All calculations were performed with the program package Gaussian 09 (revision D.01) [43].

The topological analysis of the charge density distribution was performed through means of Bader's quantum theory of atoms in molecules (QTAIM) [44] using the AIMALL [45] program package (version 17.01.25) and utilizing the SMD/M06/6-31+G(d,p) + LANL2DZ wave function obtained from the optimization.

The Gibbs free energy of the interactions, ΔG^*_{INT}, was calculated according to the formula $\Delta G^*_{INT} = G^*_{AB} - G^*_A - G^*_B$, where G^*_{AB} is the total free energy of the resulting AB structure and G^*_A and G^*_B are the total free energies of the associating units A and B, respectively. A detailed description of the computational modeling can be found in the Supplementary Materials.

2.2. Materials, Chemicals and Solutions

The substrates whose surfaces were functionalized were the titanium discs (Ti, 99.9%, ϕ = 12 mm, thickness 1.5 mm, Alfa Aesar®, Karlsruhe, Germany).

The following chemicals were used as received: sodium alendronate trihydrate (≥97%, Merck Sharp & Dohme, Rahway, NJ, USA), acetone (p.a., Gram-Mol, Zagreb, Croatia) and absolute ethanol (p.a., Gram-Mol, Zagreb, Croatia).

The powder of sodium alendronate trihydrate was dissolved in Milli-Q® water (Millipore, Merck, Darmstadt, Germany) via ultrasonic stirring for 10 min to obtain a 10 mmol dm^{-3} solution. The phosphate-buffered solution (10.0530 g $Na_2HPO_4 \cdot 7H_2O$ + 1.9501 g $NaH_2PO_4 \cdot 2H_2O$ were dissolved in 0.5 dm^3 water; pH = 7.4) was used to prepare an oxide layer on the Ti substrate. The Fusayama artificial saliva, prepared via dissolving 0.4 g NaCl, 0.4 g KCl, 0.6 g $CaCl_2 \cdot 2H_2O$, 0.58 g $Na_2HPO_4 \cdot 2H_2O$ and 1 g urea in 1 dm^3 water [46], was used as a model solution to monitor spontaneous CaP formation. All solutions were prepared with Milli-Q® water.

2.3. Functionalisation of the Titanium Samples

The titanium sample covered using electrochemically formed oxide film coated with alendronate (Ti/oxide/alendronate) was prepared.

Prior to modification, the surface of Ti samples was abraded with 240, 500 and 600 grit SiC emery paper, ultrasonically cleaned with absolute ethanol, acetone and Mili-Q® water and dried with nitrogen (99.999%, Messer®, Bad Soden, Germany). To create the oxide layer on the Ti surface (Ti/oxide), a potential of 2.5 V vs. Ag | AgCl, 3.0 mol dm^{-3} KCl was applied to the Ti in a phosphate-buffered solution for 5 h. The oxide layer formation was performed on the Ti disc, which was placed in a Teflon holder so that an area of 1 cm^2 was exposed to the electrolyte. The measurement was performed in a three-electrode cell with the Ti as the working electrode, the Ag | AgCl, 3.0 mol dm^{-3} KCl (E = 0.210 V vs. standard hydrogen electrode, SHE) as the reference and the graphite rod as the counter electrode using the Autolab 128N potentiostat/galvanostat (Metrohm Autolab BV, Utrecht, The Netherlands) controlled using Nova 2.1.6® software (Metrohm Autolab BV, Utrecht, The Netherlands). The Ti/oxide samples were then rinsed and dried with nitrogen. Functionalization with an alendronate layer was performed on the Ti sample with oxide layer (Ti/oxide), according to the following procedure. The Ti/oxide samples were immersed in the prepared alendronate solution at 22 ± 1 °C for 24 h. The functionalized samples were then dried at 70 °C for 7 h to ensure the chemical stability of the coating [47]. Samples were then rinsed with Milli-Q® water and absolute ethanol and dried in a nitrogen stream.

2.4. Spontaneous Formation of Calcium Phosphates (CaP) on the Titanium Samples

To investigate potential bioactivity of the Ti/oxide/alendronate sample, samples were immersed in the Fusayama artificial saliva (pH 6.8) at 22 ± 2 °C for a period of 100 days. After this period, white deposits were visible on the surface of the sample, which was characterized in more detail.

2.5. Characterisation of the Titanium Samples

The phase composition of the samples was recorded in the 2θ range between 10° and 90°, and 45 kV and 40 mA on the Empyrean powder X-ray diffractometer (PXRD) (Malvern Pananalytical B.V., Almelo, The Netherlands) with CuKα radiation (0.1542 mm).

Morphology and elemental analysis was performed using the field emission scanning electron microscope (FE-SEM, model JSM-7000F, Jeol Ltd., Tokyo, Japan) in conjunction with the energy dispersive X-ray analyzer EDS/INCA 350, (Oxfore Instruments, High Wycombe, UK). Micrographs were recorded at 5 kV accelerating voltage and 10 mm working distance. The EDS analysis was performed with an accelerating voltage of 10 kV, a working distance of 10 mm, acquisition time of 180 s and a dead time of 16%.

The attenuated total reflectance Fourier transform infrared (ATR-FTIR) spectra were measured with the IRTracer-100 spectrometer (Shimadzu, Kyoto, Japan) during 45 cycles in the range of 4000 to 450 cm^{-1} with a scan resolution of 4 cm^{-1}.

The results shown in this study are the average of three measurements.

3. Results and Discussion

3.1. The Mechanism of Interaction of Calcium and Phosphate Ions with Ti/Oxide/Alendronate

To gain insight into the possible interactions between calcium and phosphate ions present in body fluids with Ti/oxide/alendronate at the molecular level, a detailed theoretical study using quantum chemical DFT calculations was performed. The interaction of calcium and phosphate ions with the alendronate-coated surface was analyzed in terms of the interaction pattern and interaction energy. Herein, the aim of the theoretical simulations was not to investigate the entire nucleation route for calcium phosphate, but rather the initial stage of the aggregation of calcium and phosphate ions at the alendronate coating. The hydrogen phosphate anion HPO_4^{2-} was considered for the simulation as it is the main phosphate species present in the solution at pH = 6.5. Also, it is important to point out that the ion association process between Ca^{2+} and HPO_4^{2-} occurs immediately at the beginning of the deposition process, forming a $CaHPO_4$ ion pair which interacts with alendronate coating.

Since the TiO_2 layer is present on the titanium surface, the TiO_2 nanocluster was selected for the simulation of the metal oxide layer. For the sake of computational efficiency, the $(TiO_2)_{10}$ nanocluster used by Qu and Kroes [48] was selected to serve for cluster modeling.

Previously reported results for the alendronate–coated titanium surface [15] showed that it is most likely the result of two energetically competing structures, one in which the alendronate molecule is bound to the TiO_2 surface via both the amine and phosphonate groups, while in the other the alendronate molecule is bound only via the phosphonate group, with the former being slightly more favorable by 3.48 kcal mol^{-1}. Therefore, to model the $(TiO_2)_{10}$-alendronate-CaP structure, both $(TiO_2)_{10}$–alendronate structures are taken into account.

In the case of the more stable $(TiO_2)_{10}$–alendronate structure, the formation of the CaP deposit can be initiated by the following two structures. In one, $(TiO_2)_{10}$–alendronate–CaP–I (Figure 1a), which is more favorable, the calcium ion binds to the two phosphonate groups of the alendronate molecule, releasing the Gibbs free energy of $\Delta G^*_{INT} = -31.14$ kcal mol^{-1}.

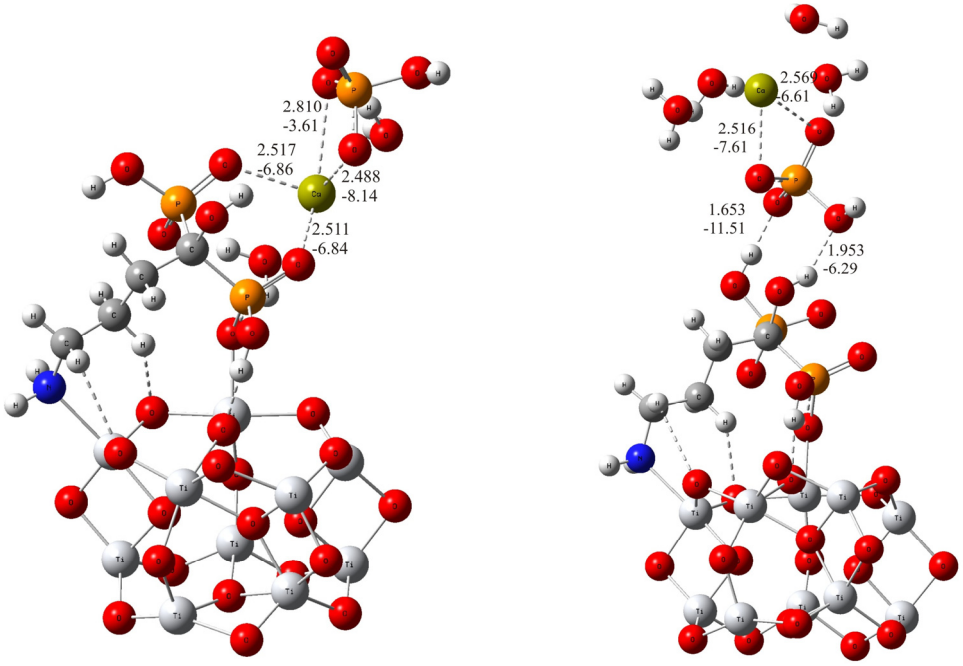

ΔG^*_{INT} = −31.14 kcal mol^{-1} ΔG^*_{INT} = −9.29 kcal mol^{-1}

(**a**) (**b**)

Figure 1. The most stable structures predicted using DFT calculations: (**a**) $(TiO_2)_{10}$–alendronate–CaP–I and (**b**) $(TiO_2)_{10}$–alendronate–CaP–II. The bond lengths are given in Å, the bond energies are given in kcal mol^{-1}. Ti—light gray, O—red, C—gray, N—blue, P—orange, H—white, Ca—yellow-green.

The interaction between the phosphonate groups and the calcium ion is achieved by two strong coordinate P–O–Ca bonds ($d_{Ca\cdots O}$ = 2.517 Å and 2.511 Å; $E_{Ca\cdots O}$ = −6.84 kcal mol^{-1} and −6.86 kcal mol^{-1}; Figure 1a), where a free electron pair from the oxygen atom of the phosphonate group of the alendronate molecule is involved in the binding with the calcium ion. In addition, the HPO_4^{2-} ion binds to the calcium ion via Ca–O bonds ($d_{Ca\cdots O}$ = 2.810 Å and 2.488 Å; $E_{Ca\cdots O}$ = −3.61 kcal mol^{-1} and −8.14 kcal mol^{-1}; Figure 1a) in bidentate fashion, and is aligned in the upper part of the $(TiO_2)_{10}$–alendronate–CaP–I structure. The formed Ca–O bonds are attributed to an ionic interaction type according to $\nabla^2\rho(rc) > 0$ and $H(rc) > 0$ from the topological analysis of the electronic density distribution. In addition, two water molecules are found in the first coordination shell of the Ca^{2+} ion.

When the formation of CaP is accomplished via the phosphate group of the $CaHPO_4$ ion pair, the considerably less stable structure ($(TiO_2)_{10}$–alendronate–CaP–II) with ΔG^*_{INT} = −9.29 kcal mol^{-1} is obtained (Figure 1b). In this structure, the phosphate group binds to the alendronate molecule at the phosphonate site via two strong hydrogen O···H–O bonds ($d_{O\cdots H}$ = 1.653 Å and 1.953 Å; $E_{O\cdots H}$ = −11.51 kcal mol^{-1} and −6.29 kcal mol^{-1}; Figure 1b). The remaining two oxygen atoms of the phosphate group coordinate the calcium in a bidentate manner ($d_{Ca\cdots O}$ = 2.516 Å and 2.569 Å; $E_{Ca\cdots O}$ = −7.61 kcal mol^{-1} and −6.61 kcal mol^{-1}; Figure 1b). The critical point of the formed Ca–O bonds was characterized by positive values of the electron density Laplacian, $\nabla^2\rho(rc) > 0$, and by a positive value of the electron energy density, $H(rc) > 0$, which assigns the Ca–O bonds to an ionic interaction type.

The calculated Gibbs free energies of the interactions for the $(TiO_2)_{10}$–alendronate–CaP structures selected above point to the spontaneous formation ($\Delta G^*_{INT} < 0$) for both structures. However, the binding is found to be much more exergonic in the case of $(TiO_2)_{10}$–alendronate–CaP–I (Figure 1a), leading to the conclusion that CaP deposition on the alendronate coatings occurs mainly through the calcium ($CaHPO_4$)–phosphonate (alendronate) interactions.

For the thermodynamically less stable but highly competitive $(TiO_2)_{10}$–alendronate structure, two modes of binding of calcium and phosphate ions to alendronate molecule are also obtained (Figure 2). In the one, thermodynamically more stable structure, the calcium and phosphate ions interact with the alendronate molecule via the calcium ion, which binds to two oxygen atoms of the phosphonate group of the alendronate molecule ($(TiO_2)_{10}$–alendronate–CaP–III, $d_{Ca\cdots O}$ = 2.478 Å and 2.450 Å; $E_{Ca\cdots O}$ = −7.50 kcal mol^{-1} and −8.11 kcal mol^{-1}; Figure 2a). The phosphate ion binds to the calcium ion via two oxygen atoms with $d_{Ca\cdots O}$ = 2.507 Å and 2.663 Å and $E_{Ca\cdots O}$ = −7.79 kcal mol^{-1} and −5.19 kcal mol^{-1}, respectively (Figure 2a). The additional interaction of the phosphate ion with the amino group is established through the strong O···H–N hydrogen bond ($d_{O\cdots H}$ = 2.192 Å; $E_{O\cdots H}$ = −4.00 kcal mol^{-1}; Figure 2a). It can be considered, according to the QTAIM analysis, as a partially ionic and partially covalent interaction in accordance with the positive value of Laplacian, $\nabla^2\rho(rc) > 0$, and the negative value of the electron energy density, $H(rc) < 0$, at the bond critical point. The Gibbs free energy of interaction for the structure under consideration is calculated as ΔG^*_{INT} = −34.65 kcal mol^{-1}.

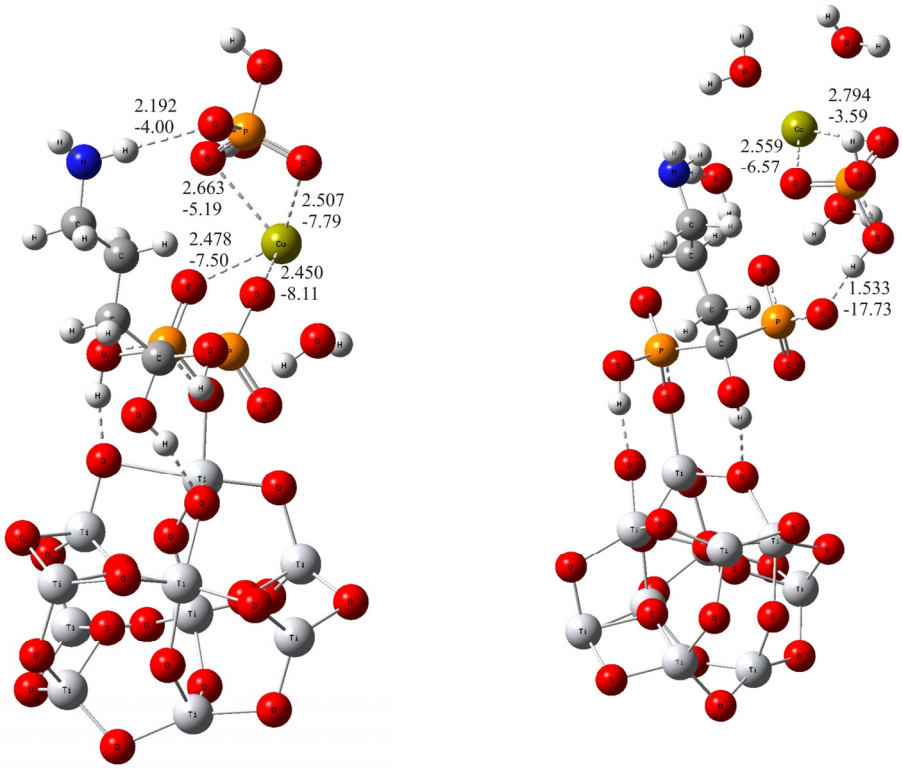

ΔG^*_{INT} = −34.65 kcal mol^{-1} ΔG^*_{INT} = −11.75 kcal mol^{-1}

(**a**) (**b**)

Figure 2. The most stable structures predicted using DFT calculations: (**a**) $(TiO_2)_{10}$–alendronate–CaP–III and (**b**) $(TiO_2)_{10}$–alendronate–CaP–IV. The bond lengths are given in Å, the bond energies are given in kcal mol^{-1}. Ti—light gray, O—red, C—gray, N—blue, P—orange, H—white, Ca—yellow-green.

In the alternative structure, $(TiO_2)_{10}$–alendronate–CaP–IV (Figure 2b), the binding of the CaP ion pair via the phosphate group, leads to a less stable structure with a Gibbs free interaction energy of −11.75 kcal mol^{-1}. In this structure, the phosphate ion of the $CaHPO_4$ ion pair interacts with the phosphonate group of the alendronate molecule, resulting in an anchoring hydrogen O···H–O bond with a corresponding bond length of 1.533 Å and an energy of $E_{O\cdots H}$ = −17.73 kcal mol^{-1}. The phosphate group coordinates the calcium ion through two bonds with a corresponding bond length of $d_{Ca\cdots O}$ = 2.559 Å and 2.794 Å and

energies of $E_{Ca\cdots O}$ = −6.57 kcal mol^{-1} and −3.59 kcal mol^{-1}, respectively (Figure 2b). It is worth mentioning that no interaction of the CaP ion pair with the NH_2 group of alendronate molecule was found.

In summary, the deposition of calcium and phosphate ions on the alendronate modified titanium oxide surface is governed by Ca^{2+}–phosphonate interaction. It is supported by the hydrogen bond between the phosphate group of CaP and the amino group of the alendronate molecule, as found in the structure $(TiO_2)_{10}$–alendronate–CaP–III. Those interactions ensure a thermodynamically strong favorable binding pattern with a released Gibbs free interaction energy of ΔG^*_{INT} = −34.65 kcal mol^{-1}.

To put the above results in perspective, the DFT calculations of the interactions of bare TiO_2 clusters with calcium phosphate ions were carried out. The most stable structure for each of the considered binding modes (analogous to the previous ones with alendronate coating) were determined and demonstrated in Figure 3.

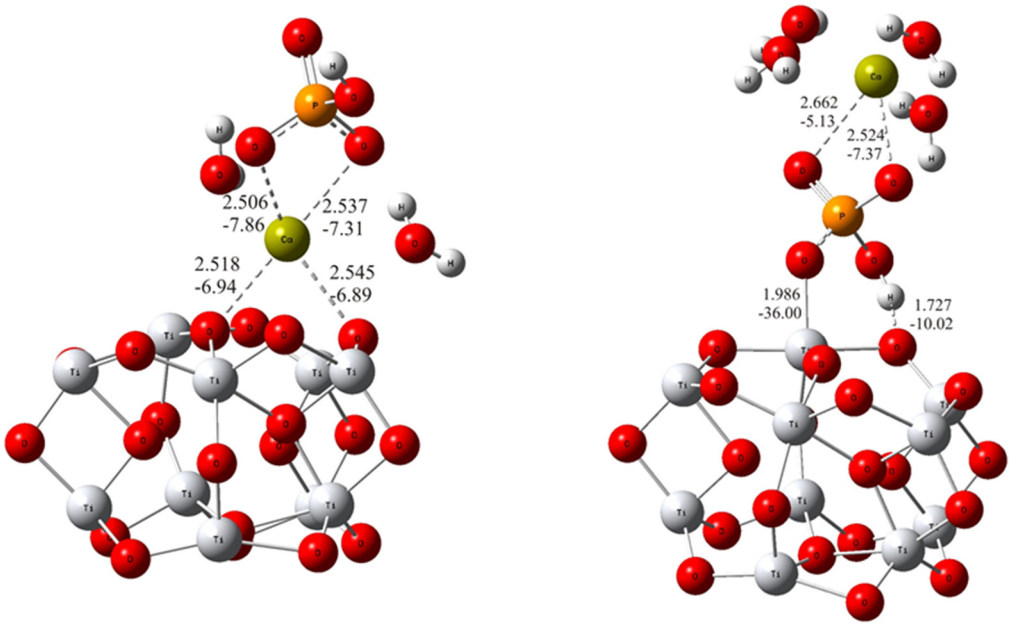

ΔG^*_{INT} = -5.28 kcal mol^{-1} (**a**)

ΔG^*_{INT} = -20.26 kcal mol^{-1} (**b**)

Figure 3. The most stable structures predicted using DFT calculations: (**a**) $(TiO_2)_{10}$–CaP–I and (**b**) $(TiO_2)_{10}$–CaP–II. The bond lengths are given in Å, the bond energies are given in kcal mol^{-1}. Ti—light gray, O—red, C—gray, P—orange, H—white, Ca—yellow-green.

As can be seen from the DFT results, the binding established through the interaction of the phosphate ion of CaP (ΔG^*_{INT} = −20.26 kcal mol^{-1}; Figure 3b) with the TiO_2 surface is more exergonic than the binding achieved through the Ca^{2+} – $O_{(TiO2)10}$ (ΔG^*_{INT} = −5.28 kcal mol^{-1}; Figure 3a) interactions. However, compared to the most favorable binding of calcium phosphate ions to the alendronate modified titanium oxide surface, it appeared significantly less exergonic ($\Delta(\Delta G^*_{INT})$ = 14.39 kcal mol^{-1}). These findings clearly indicate the positive effects of alendronate coating on the formation of CaP which is fully in line with the experimental observations.

3.2. Experimental Evidence for the Spontaneous Formation of Calcium Phosphates (CaP) on the Ti/oxide/Alendronate Surface

Since the DFT results clearly showed that the spontaneous formation of CaP on the alendronate-modified Ti/oxide surface is possible, experimental evidence was obtained using SEM, EDS, ATR-FTIR and XRD techniques. The prepared Ti/oxide/alendronate sam-

ples were immersed for 100 days in Fusayama artificial saliva solution as simulated body fluid to test alendronate coating's bioactivity on the basis of monitoring the spontaneous CaP deposit formation.

Morphology, Chemical and Phase Analysis of Ti/Oxide/Alendronate Samples after 100 Days Immersion in Artificial Saliva

SEM measurements were performed to gain insight into the morphology of the Ti/oxide/alendronate sample before and after immersion in the artificial saliva for 100 days. The results are shown in Figure 4. The inhomogeneous-layered structure is evident for the Ti/oxide/alendronate surface (Figure 4a), as a consequence of the presence of electrochemically prepared oxide film on the Ti surface. It is well-known that the alendronate coating has no significant effect on the morphology due to its low thickness (one monolayer) [47].

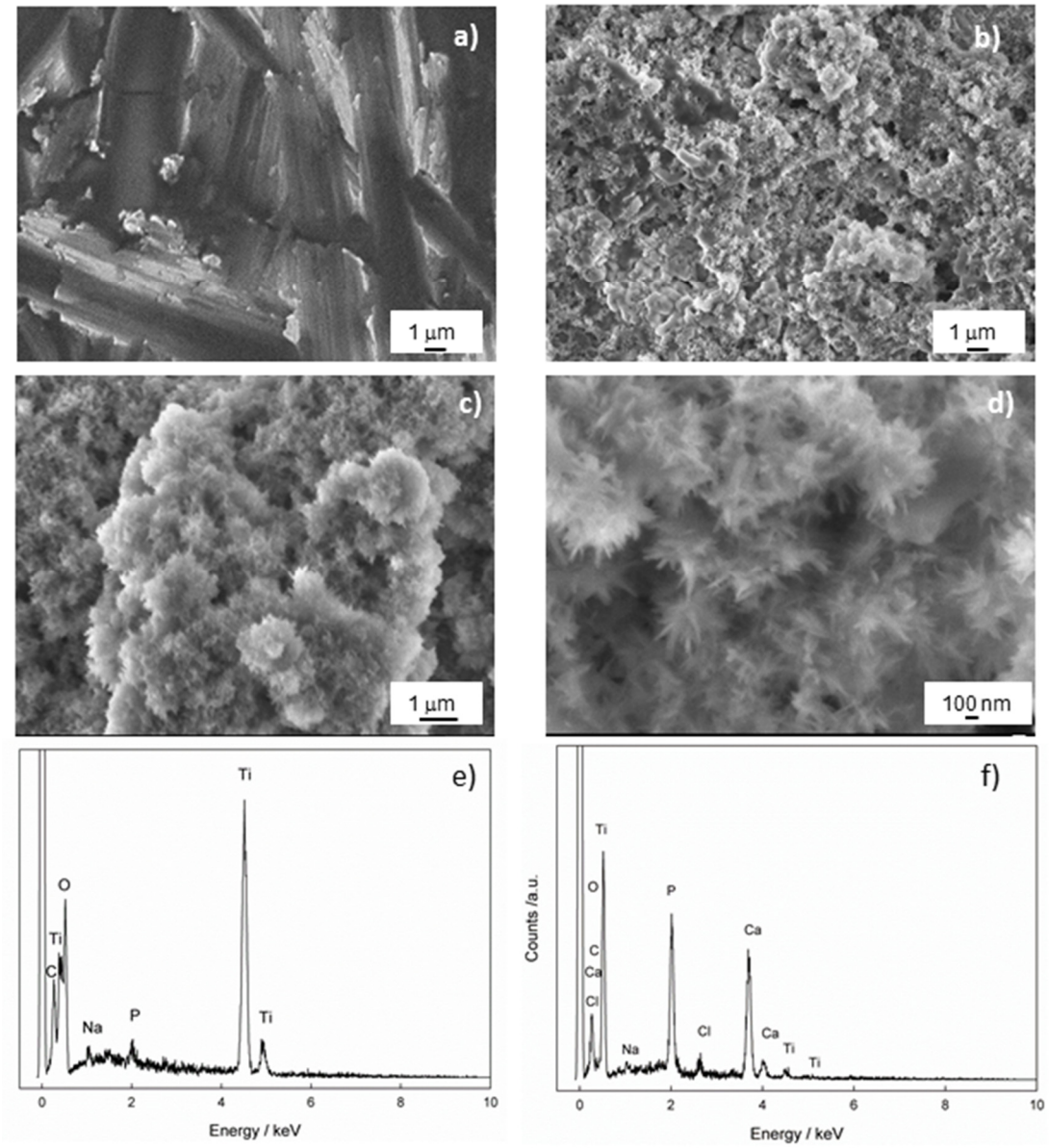

Figure 4. The FE-SEM images of Ti/oxide/alendronate (**a**) before and (**b**–**d**) after immersion in artificial saliva. The images were taken at (**a**,**b**) 5000×, (**c**) 10,000× and (**d**) 33,000× magnification. The chemical composition of the Ti/oxide/alendronate sample (**e**) before and (**f**) after immersion in artificial saliva.

The immersion of the sample in the artificial saliva over a period of 100 days changed the morphology of the Ti/oxide/alendronate surface significantly and resulted in the spontaneous formation of agglomerates over almost the entire surface (Figure 4b,c). A deeper look into the spontaneously formed deposit (Figure 4d) revealed a flower agglomerate consisting of nanoneedles. The morphology obtained is one of the possible forms of CaP structures such as nanosheets, microrods, and microplates, which are influenced by the precipitation conditions (temperature, pH, reactants and their concentrations) [49,50]. Nanoneedles are also observed under similar pH conditions [50–52].

To check the chemical composition of the Ti/oxide/alendronate sample before and after immersion in artificial saliva, the samples were analyzed using EDS. The results are shown in Table 1 and Figure 4e,f, and indicate that the alendronate coating (Na and P were detected) was present over the oxide layer on the titanium before immersion in artificial saliva. As can be seen after 100 days of immersion, the elements Na, Ca, P and Cl were detected on the surface of the sample, whereby the amount of the element P increased significantly and the other elements Ca and Cl were incorporated into the structure of the deposit (Table 1). The Ca/P atomic ratio is 1.51 and may indicate the presence of calcium-deficient hydroxyapatite (CDHAp) [53]. Furthermore, due to the presence of the elements Cl and Na, it can be concluded that the apatite formed is biocompatible, closely resembling the natural bone composition, which could have a positive effect on bone metabolism [54].

Table 1. Chemical composition of the Ti/oxide/alendronate sample before and after the immersion in artificial saliva (the average of three measurements).

	Element, at. %						
Sample	**Ti K**	**C K**	**O K**	**Na K**	**P K**	**Ca K**	**Cl K**
Before immersion	40.76	12.18	45.16	0.99	0.91	/	/
After immersion	1.41	16.68	54.22	0.49	10.41	15.74	1.05

It should be emphasized that atmospheric carbon contamination is possible, which could influence the EDS results. The prompt gamma-ray activation analysis (PGAA) can be useful for the accurate determination of elemental composition, as shown by A. Nespoli et al. [55].

The surface characterization (composition) of Ti/oxide/alendronate samples before and after immersion was performed using ATR-FTIR (Figure 5). Prior to sample immersion, weak bands around 1000 cm^{-1} are visible characteristics for the P–O and P=O bands present in the alendronate molecule [16,56,57]. On the other hand, after immersion bands were detected in the spectral range from 900 to 1100 cm^{-1}, typical for the symmetric and asymmetric P–O stretching modes in the phosphate group [58–60]. The noticeable strong bands are indicative of phosphate layer deposits; i.e., dominant ν_3 PO_4^{3-} absorption bands in the range 1080–1000 cm^{-1} (P–O asymmetric stretching vibrations), the ν_1 PO_4^{3-} band at 961 cm^{-1} (P–O symmetric stretching vibrations) and the bending mode bands (O–P–O vibrations) in range from 560 to 630 cm^{-1} [58–60]. The visible band at 1645 cm^{-1} is assigned to the ν_2 bending mode of adsorbed water associated with the hydroxyapatite phase [58], accompanied with bands at 3456 and 3344 cm^{-1} typical for the hydroxyl stretching present in hydroxyapatite [59].

Additionally, the bands at 1464, 862 and 774 cm^{-1} are attributed to the ν_1 CO_3^{2-} band (asymmetric stretching mode of carbonate group), the ν_2 CO_3^{2-} band (symmetric stretching mode of carbonate group) and the ν_4 CO_3^{2-} band (asymmetric stretching mode of carbonate group) and point to the carbonate content present in the calcium phosphate deposit [58,59], which is due to the atmospheric conditions during spontaneous deposition. Carbonate ions replace hydroxyl or phosphate ions in the hydroxyapatite coating, resulting in the formation of calcium-deficient hydroxyapatite with a decreased Ca/P ratio in comparison to the Ca/P ratio of hydroxyapatite [21]. This was the case for the deposit investigated, with the Ca/P ratio of 1.51. Hence, the results obtained are in accordance with the SEM/EDS

results discussed previously in this section. The detected carbonate content should not be considered detrimental or unwanted since it allows for a closer resemblance to the natural bone composition [22,61].

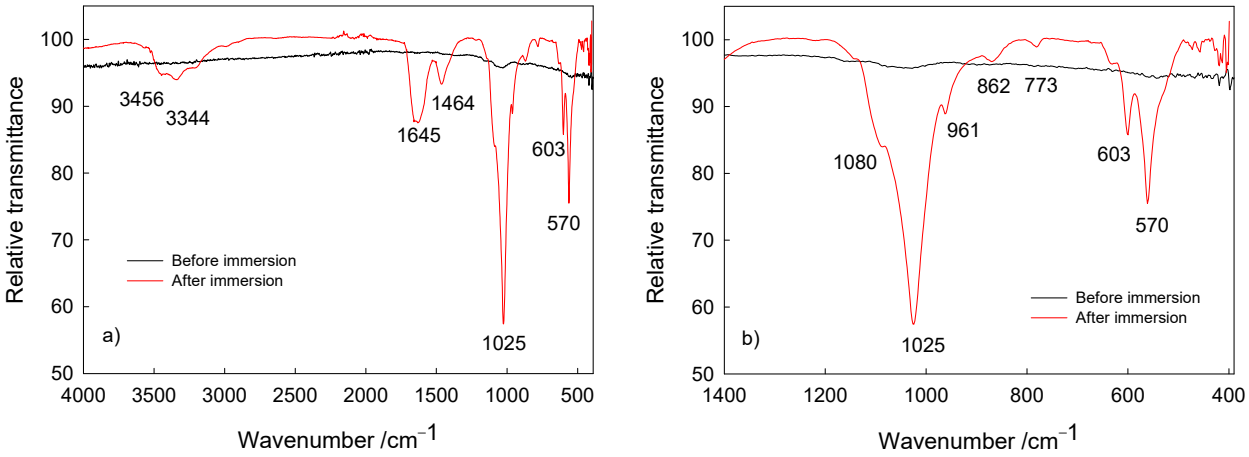

Figure 5. The ATR-FTIR of Ti/oxide/alendronate before and after immersion in artificial saliva: (**a**) wide range spectra and (**b**) P–O bands in the fingerprint region of the spectra.

The obtained ATR-FTIR spectra confirm the spontaneous formation of a calcium phosphate deposit on the Ti/oxide/alendronate sample during immersion in the artificial saliva solution, corroborating the enhanced bioactivity of the titanium implant material upon alendronate coating formation.

The phase analysis of the samples before and after immersion in artificial saliva solution was performed using XRD and the results are shown in Figure 6. Figure 6a shows the XRD data for the Ti/oxide/alendronate before immersion in artificial saliva solution. The comparison of the experimental data with the reference card for titanium (JCPDS #00-044-1294) [62] clearly shows the dominance of the titanium substrate as a single phase. Since the electrochemically formed oxide layer is obviously very thin, the oxide phase was not detected in the XRD pattern.

The XRD pattern of the Ti/oxide/alendronate sample after immersion in artificial saliva solution contains characteristic peaks for hydroxyapatite (HAp, JCPDS # 00-009-0432) [53] and beta-tricalcium phosphate (β-TCP, JCPDS # 00-009-0169) [21,63], (Figure 6b,c). The peaks of the titanium substrate are also visible. The results are in accordance with the ATR-FTIR results. The experimental conditions (artificial saliva with a pH of 6.5, room temperature and 100 days immersion) lead to the formation of a mixture of β-TCP and HAp in the form of floral deposits of nanoneedles. The result is consistent with the EDS results, where the Ca/P ratio also indicates the formation of HAp, i.e., calcium-deficient HAp. The formed mixture of HAp and β-TCP can be very useful from an application point of view, as this combination is an important material for tissue engineering and a process of bone formation [64].

In summary, the formation of calcium-deficient hydroxyapatite was spontaneously induced on the titanium covered with electrochemically prepared oxide film and was subsequently modified by the alendronate coating, as was validated using XRD, EDS and ATR-FTIR characterization methods. Spontaneous formation points to the bioactivity of the alendronate coating, resulting in the development of a calcium phosphate phase with beneficial properties. Since, the presence of hydroxyapatite plays a crucial role in various phases of new bone growth, including cell adhesion, the bone formation phase, also serving as a scaffold for new bone deposition, the mineralization phase and bone remodeling, its presence facilitates and is the essential for the successful implant integration [21–24].

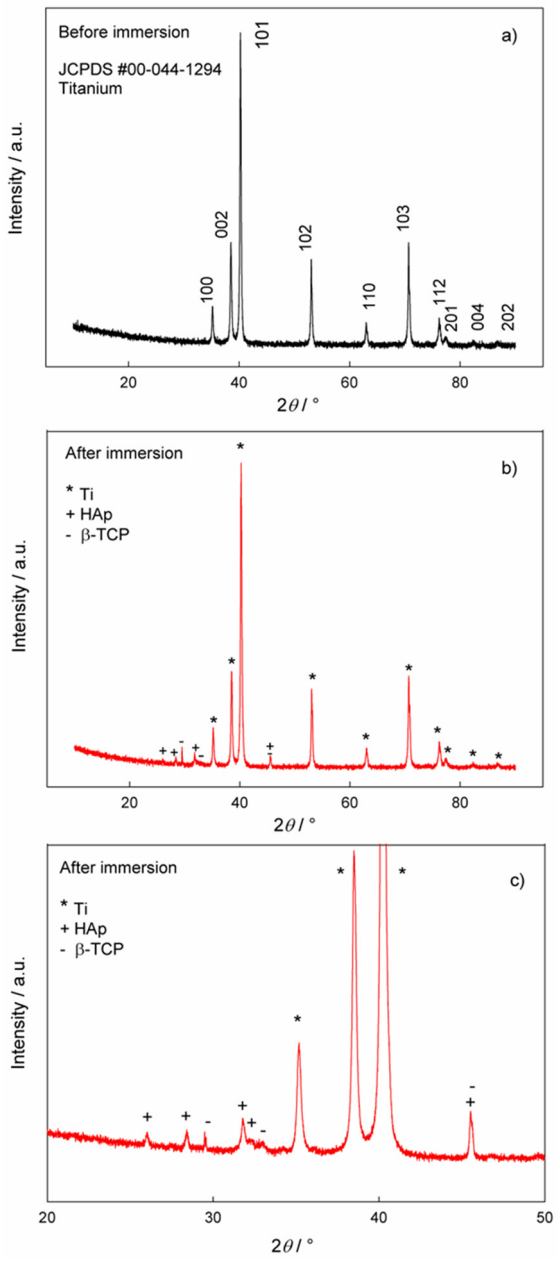

Figure 6. The XRD patterns of the Ti/oxide/alendronate sample (**a**) before and (**b**,**c**) after immersion in artificial saliva. (**c**) Pattern from figure (**b**) in the narrower 2θ region, 20–50°.

4. Conclusions

In this study, the spontaneous calcium phosphate deposition onto an alendronate modified TiO_2 surface was investigated both in silico by means of DFT quantum chemical calculations and in vitro by a simple immersion procedure in artificial saliva.

The DFT results showed that the molecular interactions between the alendronate–coated Ti/oxide surface and the calcium and phosphate ions were spontaneous according to the calculated negative Gibbs free interaction energy. It has been shown that the deposition of calcium and phosphate ions on the alendronate-modified titanium surface is determined by the interaction of Ca^{2+} with the phosphonate group (-PO_3H) of the alendronate molecule and is strongly supported by the O···H–N hydrogen bonding between the phosphate (HPO_4^{2-}) and the amino group (-NH_2) of the alendronate molecule. The formation of the most stable $(TiO_2)_{10}$–alendronate–CaP structure proves to be a highly exergonic process with a calculated Gibbs free interaction energy of $\Delta G^*_{INT} = -34.65$ kcal mol^{-1}.

The results of scanning electron microscopy, energy dispersive X-ray spectroscopy and attenuated total reflectance Fourier transform infrared spectroscopy confirmed spontaneous calcium phosphate deposition on the Ti/oxide/alendronate surface after 100 days of exposure of the sample to artificial saliva. The spontaneously formed deposit is a mixture of two phases, beta-tricalcium phosphate and calcium-deficient hydroxyapatite, according to the X-ray diffraction phase analysis. The presence of trace elements (Na, Cl) and carbonate ions in the hydroxyapatite structure, detected using energy dispersive X-ray spectroscopy and attenuated total reflectance Fourier transform infrared spectroscopy, indicates the biological hydroxyapatite, which is also confirmed by the Ca/P ratio of 1.51 (energy dispersive X-ray spectroscopy).

These results indicate the potential bioactivity of functionalized titanium and provide fundamental information useful for the development of dental implants with improved osseointegrity. For further clinical testing, biological studies in a medium similar to the complex oral environment followed by in vivo studies are required.

Supplementary Materials: The following supporting information can be downloaded at: https://www.mdpi.com/article/10.3390/ma17112703/s1, Computational modeling, Figure S1: Optimized structures of the selected systems (bond distances in Å, bond energies in kcal mol^{-1}), Table S1: Formation of CaP layer. Standard state (1M) free energies of interaction ΔrG^*_{INT} computed by using the SMD solvation model at the M06/6-311++G(2df,2pd) + LANL2DZ// M06/6-31+G(d,p) + LANL2DZ level of theory (in kcal mol^{-1}), Table S2: Total electronic energy, E^{Tot}_{soln}, obtained at the SMD/M06/6-311++G(2df,2pd) + LANL2DZ//SMD/M06/6-31+G(d,p) + LANL2DZ level of theory, thermal correction to the Gibbs free energy, $\Delta G^*_{VRT,soln}$, obtained at the SMD/M06/6-31+G(d,p) + LANL2DZ level of theory, and total free energy, G^*_X, ($G^*_X = E^{Tot}_{soln} + \Delta G^*_{VRT,soln}$) in water media of the investigated species (all energies in hartree), Table S3: Bond lengths (d), energies (E) and QTAIM properties of the selected bonds in the investigated systems, Cartesian coordinates of the calculated systems. Refs. [65–75] are cited in the Supplementary Materials.

Author Contributions: Conceptualization, I.D.; methodology, I.D., Ž.P. and J.K.; software, I.D.; validation, I.D., Ž.P. and J.K.; formal analysis, I.D., J.K. and Ž.P.; investigation, I.D., Ž.P. and D.M.; resources, I.D. and Ž.P.; data curation, I.D. and Ž.P.; writing—original draft preparation, I.D., J.K. and Ž.P.; writing—review and editing, I.D., Ž.P. and J.K.; visualization, I.D., Ž.P. and J.K.; supervision, I.D., Ž.P. and J.K.; project administration, I.D.; funding acquisition, I.D. and Ž.P. All authors have read and agreed to the published version of the manuscript.

Funding: This research was partially funded by the Croatian Academy of Sciences and Arts Foundation for 2023: "Mechanism of hydroxyapatite layer formation on the surface of a titanium implant modified with an organic nano-coating".

Institutional Review Board Statement: Not applicable.

Informed Consent Statement: Not applicable.

Data Availability Statement: The original contributions presented in the study are included in the article/Supplementary Materials, further inquiries can be directed to the corresponding authors.

Acknowledgments: The authors would like to thank the Zagreb University Computing Centre (SRCE) for generously granting computational resources on the ISABELLA cluster (isabella.srce.hr). The authors would like to thank Đurđica Brlek for her technical support with the XRD measurements.

Conflicts of Interest: The authors declare no conflicts of interest.

References

1. Brunete, D.M.; Tangvall, P.; Textor, M.; Thomsen, P. *Titanium in Medicine*, 1st ed.; Springer: Berlin, Germany, 2001.
2. Salernitano, E.; Migliaresi, C. Composite Materials for Biomedical Applications: A Review. *J. Appl. Biomater. Biomech.* **2003**, *1*, 3–18. [CrossRef] [PubMed]
3. Breme, J.; Biehl, V.; Hoffman, A. Tailor-Made Composites Based on Titanium for Medical Devices. *Adv. Eng. Mater.* **2000**, *2*, 270–275. [CrossRef]
4. Ngadiman, N.H.A.; Saman, M.Z.M. A Comprehensive Review of Biomaterials and Its Characteristics for Bone Tissue Engineering Scaffold. *J. Med. Device Technol.* **2023**, *2*, 56–62. [CrossRef]

5. Qu, H.; Fu, H.; Han, Z.; Sun, Y. Biomaterials for bone tissue engineering scaffolds: A review. *RSC Adv.* **2019**, *45*, 26252–26262. [CrossRef] [PubMed]
6. Wu, H.; Chen, X.; Kong, L.; Liu, P. Mechanical and Biological Properties of Titanium and Its Alloys for Oral Implant with Preparation Techniques: A Review. *Materials* **2023**, *16*, 6860. [CrossRef] [PubMed]
7. Hanawa, T. Biocompatibility of titanium from the viewpoint of its surface. *Sci. Technol. Adv. Mater.* **2022**, *23*, 457–472. [CrossRef] [PubMed]
8. Chen, Q.; Thouas, G.A. Metallic implant biomaterials. *Mater. Sci. Eng. R* **2015**, *87*, 1–57. [CrossRef]
9. Kaur, M.; Singh, K. Review on titanium and titanium-based alloys as biomaterials for orthopaedic applications. *Mater. Sci. Eng. C* **2019**, *102*, 844–862. [CrossRef] [PubMed]
10. Xue, T.; Attarilar, S.; Liu, S.; Liu, J.; Song, X.; Li, L.; Zhao, B.; Tang, Y. Surface Modification Techniques of Titanium and its Alloys to Functionally Optimize Their Biomedical Properties: Thematic Review. *Front. Bioeng. Biotechnol.* **2020**, *8*, 603072. [CrossRef]
11. Petrović, Ž.; Katić, J.; Šarić, A.; Despotović, I.; Matijaković, N.; Kralj, D.; Leskovac, M.; Petković, M. Influence of Biocompatible Coating on Titanium Surface Characteristics. *ICMS* **2020**, *10*, 37–46. [CrossRef]
12. Vyas, V.; Kaur, T.; Kar, S.; Thirugnanam, A. Biofunctionalization of commercially pure titanium with chitosan/hydroxyapatite biocomposite via silanization: Evaluation of biological performances. *J. Adhes. Sci. Technol.* **2017**, *31*, 1768–1781. [CrossRef]
13. Sharma, A.; Kokil, G.R.; He, Y.; Lowe, B.; Salam, A.; Altalhi, T.A.; Ye, Q.; Kumeria, T. Inorganic/organic combination: Inorganic particles/polymer composites for tissue engineering applications. *Bioact. Mater.* **2023**, *24*, 535–550. [CrossRef]
14. Nayak, G.S.; Carradò, A.; Masson, P.; Pourroy, G.; Mouillard, F.; Migonney, V.; Falentin-Daudre, C.; Pereira, C.; Palkowski, H. Trends in Metal-Based Composite Biomaterials for Hard Tissue Applications. *JOM* **2022**, *74*, 102–125. [CrossRef]
15. Petrović, Ž.; Šarić, A.; Despotović, I.; Katić, J.; Peter, R.; Petravić, M.; Petković, M. A New Insight into Coating's Mechanism Between TiO_2 and Alendronate on Titanium Dental Implant. *Materials* **2020**, *13*, 3220. [CrossRef]
16. Petrović, Ž.; Šarić, A.; Despotović, I.; Katić, J.; Peter, R.; Petravić, M.; Ivanda, M.; Petković, M. Surface Functionalisation of Dental Implants with a Composite coating of Alendronate and Hydrolysed Collagen: DFT and EIS Studies. *Materials* **2022**, *15*, 5127. [CrossRef]
17. Rojo, L.; Gharibi, B.; McLister, R.; Meenan, B.; Deb, S. Self-assembled monolayers of alendronate on Ti_6Al_4V alloy surfaces enhance osteogenesis in mesenchymal stem cells. *Sci. Rep.* **2016**, *6*, 30548. [CrossRef] [PubMed]
18. Meraw, S.J.; Reeve, C.M.; Wollan, P.C. Use of alendronate in peri-implant defect regeneration. *J. Periodontol.* **1999**, *70*, 151–158. [CrossRef] [PubMed]
19. Meraw, S.J.; Reeve, C.M. Qualitative analysis of peripheral peri-implant bone and influence of alendronate sodium on early bone regeneration. *J. Periodontol.* **1999**, *70*, 1228–1233. [CrossRef]
20. Abtahi, J.; Tengvall, P.; Aspenberg, P. A bisphosphonate-coating improves the fixation of metal implants in human bone. A randomized trial of dental implants. *Bone* **2012**, *50*, 1148–1151. [CrossRef]
21. Eliaz, N.; Metoki, N. Calcium Phosphate Bioceramics: A Review of Their History, Structure, Properties, Coating Technologies and Biomedical Applications. *Materials* **2017**, *10*, 334. [CrossRef]
22. Jeong, J.; Kim, J.H.; Shim, J.H.; Hwanf, N.S.; Heo, C.Y. Bioactive calcium phosphate materials and applications in bone regeneration. *Biomater. Res.* **2019**, *23*, 4. [CrossRef] [PubMed]
23. Xiao, D.; Zhang, J.; Zhang, C.; Barbieri, D.; Yuan, H.; Moroni, L.; Feng, G. The role of calcium phosphate surface structure in osteogenesis and the mechanisms involved. *Acta Biomater.* **2020**, *106*, 22–33. [CrossRef] [PubMed]
24. Hou, X.; Zhang, L.; Zhou, Z.; Luo, X.; Wang, T.; Zhao, X.; Lu, B.; Chen, F.; Zheng, L. Calcium Phosphate-Based Biomaterials for Bone Repair. *J. Funct. Biomater.* **2022**, *13*, 187. [CrossRef] [PubMed]
25. Liu, Q.; Ding, J.; Mante, F.K.; Wunder, S.L.; Baran, G.R. The role of surface functional groups in calcium phosphate nucleation on titanium foil: A self-assembled monolayer technique. *Biomaterials* **2002**, *23*, 3103–3111. [CrossRef] [PubMed]
26. Li, H.; Huang, W.; Zhang, Y.; Zhong, M. Biomimetic synthesis of enamel-like hydroxyapatite on self-assembled monolayers. *Mater. Sci. Eng. C* **2007**, *27*, 756–761. [CrossRef]
27. Majewski, P.J.; Allidi, G. Synthesis of hydroxyapatite on titanium coated with organic self-assembled monolayers. *Mater. Sci. Eng. A* **2006**, *420*, 13–20. [CrossRef]
28. Tanahashi, M.; Matsuda, T. Surface functional group dependence on apatite formation on self-assembled monolayers in a simulated body fluid. *J. Biomed. Mater. Res.* **1997**, *34*, 305–315. [CrossRef]
29. Zeller, A.; Musyanovych, A.; Kappl, M.; Ethirajan, A.; Dass, M.; Markova, D.; Klapper, M.; Landfester, K. Nanostructured Coatings by Adhesion of Phosphonated Polystyrene Particles onto Titanium Surface for Implant Material Applications. *ACS Appl. Mater. Interfaces* **2010**, *2*, 2421–2428. [CrossRef] [PubMed]
30. Liu, L.; Zheng, Y.; Zhang, Q.; Yu, L.; Hu, Z.; Liu, Y. Surface phosphonation treatment shows dose-dependent enhancement of the bioactivity of polyetheretherketone. *RSC Adv.* **2019**, *9*, 30076–30086. [CrossRef]
31. Chang, R.; Liu, Y.-J.; Zhang, Y.-L.; Zhang, S.-Y.; Han, B.-B.; Chen, F.; Chen, Y.-X. Phosphorylated and Phosphonated Low-Complexity Protein Segments for Biomimetic Mineralization and Repair of Tooth Enamel. *Adv. Sci.* **2022**, *9*, 2103829. [CrossRef]
32. Liu, C.; Liu, C.; Gao, Y.; Cheng, F.; Xiao, G.G.; Wang, J.; Jian, X. Apatite Formation on Poly(aryl ether sulfone ketone) Surfaces by Means of Polydopamine Layers Functionalized with Phosphonate Groups. *Adv. Mater. Interfaces* **2018**, *5*, 1800003. [CrossRef]

33. Tan, G.; Ouyang, K.; Wang, H.; Zhou, L.; Wang, X.; Liu, Y.; Zhang, L.; Ning, C. Effect of Amino-, Methyl- and Epoxy-Silane Coupling as a Molecular Bridge for Formatting a Biomimetic Hydroxyapatite Coating on Titanium by Electrochemical Deposition. *J. Mater. Sci. Technol.* **2016**, *32*, 956–965. [CrossRef]
34. Yakufu, M.; Wang, Z.; Wang, Y.; Jiao, Z.; Guo, M.; Liu, J.; Zhang, P. Covalently functionalized poly(etheretherketone) implants with osteogenic growth peptide (OGP) to improve osteogenesis activity. *RSC Adv.* **2020**, *10*, 9777–9785. [CrossRef] [PubMed]
35. Sánchez-Bodón, J.; Andrade Del Olmo, J.; Alonso, J.M.; Moreno-Benítez, I.; Vilas-Vilela, J.L.; Pérez-Álvarez, L. Bioactive Coatings on Titanium: A Review on Hydroxylation, Self-Assembled Monolayers (SAMs) and Surface Modification Strategies. *Polymers* **2021**, *31*, 165. [CrossRef] [PubMed]
36. Zhao, Y.; Thrular, D.G. The M06 suite of density functionals for main group thermochemistry, thermochemical kinetics, noncovalent interactions, excited states, and transition elements: Two new functionals and systematic testing of four M06-class functionals and 12 other functionals. *Theor. Chem. Acc.* **2008**, *120*, 215–241. [CrossRef]
37. Zhao, Y.; Truhlar, D.G. Density Functionals with Broad Applicability in Chemistry. *Acc. Chem. Res.* **2008**, *41*, 157–167. [CrossRef] [PubMed]
38. Zhao, Y.; Truhlar, D.G. Density Functional Theory for Reaction Energies: Test of Meta and Hybrid Meta Functionals, Range-Separated Functionals, and Other High-Performance Functionals. *J. Chem. Theory Comput.* **2011**, *7*, 669–676. [CrossRef]
39. Wadt, W.R.; Hay, P.J. Ab initio effective core potentials for molecular calculations. Potentials for main group elements Na to Bi. *J. Chem. Phys.* **1985**, *82*, 284–298. [CrossRef]
40. Marenich, A.V.; Cramer, C.J.; Truhlar, D.G. Universal Solvation Model Based on Solute Electron Density and on a Continuum Model of the Solvent Defined by the Bulk Dielectric Constant and Atomic Surface Tensions. *J. Phys. Chem. B* **2009**, *113*, 6378–6396. [CrossRef]
41. Srinivasa Rao, J.; Dinadayalane, T.C.; Leszczynski, J.; Sastry, N. Comprehensive Study on the Solvation of Mono- and Divalent Metal Cations: Li^+, Na^+, K^+, Be^{2+}, Mg^{2+} and Ca^{2+}. *J. Phys. Chem. A* **2008**, *112*, 12944–12953. [CrossRef]
42. Pliego, J.R.; Riveros, J.M. The Cluster-Continuum Model for the Calculation of the Solvation Free Energy of Ionic Species. *J. Phys. Chem. A* **2001**, *105*, 7241–7247. [CrossRef]
43. Frisch, M.J.; Trucks, G.W.; Schlegel, H.B.; Scuseria, G.E.; Robb, M.A.; Cheeseman, J.R.; Scalmani, G.; Barone, V.; Mennucci, B.; Petersson, G.A.; et al. *Gaussian 09, Revision D.01*; Gaussian, Inc.: Wallingford, CT, USA, 2013.
44. Bader, R.F.W. *Atoms in Molecules: A Quantum Theory*; Oxford University Press: Oxford, NY, USA, 1994.
45. Keith, T.A. *AIMAll, Version 17.01.25*; TK Gristmill Software; Overland Park: Johnson County, KS, USA, 2017. Available online: https://aim.tkgristmill.com/ (accessed on 18 January 2024).
46. Mellado-Valero, A.; Muñoz, A.I.; Pina, V.G.; Sola-Ruiz, M.F. Electrochemical Behaviour and Galvanic Effects of Titanium Implants Coupled to Metallic Suprastructures in Artificial Saliva. *Materials* **2018**, *11*, 171. [CrossRef] [PubMed]
47. Katić, J.; Šarić, A.; Despotović, I.; Matijaković, N.; Petković, M.; Petrović, Ž. Bioactive Coating on Titanium Dental Implants for Improved Anticorrosion Protection: A Combined Experimental and Theoretical Study. *Coatings* **2019**, *9*, 612. [CrossRef]
48. Qu, Z.; Kroes, G.-J. Theoretical Study of Stable, Defect-Free (TiO_2)n Nanoparticles with n = 10−16. *J. Phys. Chem. C* **2007**, *111*, 16808–16817. [CrossRef]
49. Katić, J.; Krivačić, S.; Petrović, Ž.; Mikić, D.; Marciuš, M. Titanium Implant Alloy Modified by Electrochemically Deposited Functional Bioactive Calcium Phosphate Coatings. *Coatings* **2023**, *13*, 640. [CrossRef]
50. Dorozhkin, S.V. Calcium orthophosphate deposits: Preparation, properties and biomedical applications. *Mater. Sci. Eng. C* **2015**, *55*, 272–326. [CrossRef] [PubMed]
51. Lu, X.; Wang, Y.; Wang, J.; Qu, S.; Weng, J.; Xin, R.; Leng, Y. Calcium phosphate crystal growth under controlled environment through urea hydrolysis. *J. Cryst. Growth* **2006**, *297*, 396–402. [CrossRef]
52. Kobayashi, T.; Ono, S.; Hirakura, S.; Oaki, Y.; Imai, H. Morphological variation of hydroxyapatite grown in aqueous solution based on simulated body fluid. *CrystEngComm* **2012**, *14*, 1143–1149. [CrossRef]
53. Beaufils, S.; Rouillon, T.; Millet, P.; Le Bideau, J.; Weiss, P.; Chopart, J.P.; Daltin, A.L. Synthesis of calcium-deficient hydroxyapatite nanowires and nanotubes performed by template-assisted electrodeposition. *Mater. Sci. Eng. C* **2019**, *98*, 333–346. [CrossRef]
54. Lin, K.; Zhou, Y.; Zhou, Y.; Qu, H.; Chen, F.; Zhu, Y.; Chang, J. Biomimetic hydroxyapatite porous microspheres with co-substituted essential trace elements: Surfactant-free hydrothermal synthesis, enhanced degradation and drug release. *J. Mater Chem* **2011**, *21*, 16558–16565. [CrossRef]
55. Nespoli, A.; Passaretti, F.; Szentmiklósi, L.; Maróti, B.; Placidi, E.; Cassetta, M.; Yada, R.Y.; Farrar, D.H.; Tian, K.V. Biomedical NiTi and β-Ti Alloys: From Composition, Microstructure and Thermo-Mechanics to Application. *Metals* **2022**, *12*, 406. [CrossRef]
56. Ochiuz, L.; Grigoras, C.; Popa, M.; Stoleriu, I.; Munteanu, C.; Timofte, D.; Profire, L.; Grigoras, A.G. Alendronate-Loaded Modified Drug Delivery Lipid Particles Intended for Improved Oral and Topical Administration. *Molecules* **2016**, *21*, 858. [CrossRef] [PubMed]
57. Albano, C.S.; Gomes, A.M.; da Silva Feltran, G.; da Costa Fernandes, C., Jr.; Trino, L.D.; Zambuzzi, W.F.; Lisboa-Filho, P.N. Biofunctionalization of titanium surfaces with alendronate and albumin modulates osteoblast performance. *Heliyon* **2020**, *6*, e04455. [CrossRef] [PubMed]
58. Koutsopoulos, S. Synthesis and characterization of hydroxyapatite crystals: A review study on the analytical methods. *J. Biomed. Mater. Res.* **2002**, *62*, 600–612. [CrossRef] [PubMed]

59. Berzina-Cimdina, L.; Borodajenko, N. Research of Calcium Phosphates Using Fourier Transform Infrared Spectroscopy. In *Infrared Spectroscopy—Materials Science, Engineering and Technology*; Theophanides, T., Ed.; IntechOpen: Rijeka, Croatia, 2012; pp. 123–148.
60. Chukanov, N.V.; Chervonnyi, A.D. IR Spectra of Minerals and Related Compounds, and Reference Samples' Data. In *Infrared Spectroscopy of Minerals and Related Compounds*; Chukanov, N.V., Chervonnyi, A.D., Eds.; Springer: Cham, Switzerland, 2015; pp. 51–1047.
61. LeGeros, R.Z. Calcium Phosphate-Based Osteoinductive Materials. *Chem. Rev.* **2008**, *108*, 4742–4753. [CrossRef] [PubMed]
62. Han, M.-K.; Im, J.-B.; Hwang, M.-J.; Kim, B.-J.; Kim, H.-Y.; Park, Y.-J. Effect of Indium Content on the Microstructure, Mechanical Properties and Corrosion Behavior of Titanium Alloys. *Metals* **2015**, *5*, 850–862. [CrossRef]
63. Lee, S.W.; Kim, Y.; Rho, H.T.; Kim, S. Microhardness and microstructural properties of a mixture of hydroxyapatite and b-tricalcium phosphate. *J. Asian Ceram. Soc.* **2023**, *11*, 11–17. [CrossRef]
64. Vallet-Regı', M.; Gonza'lez-Calbet, J.M. Calcium phosphates as substitution of bone tissues. *Prog. Solid State Chem.* **2004**, *32*, 1–31. [CrossRef]
65. Allard, M.M.; Merlos, S.N.; Springer, B.N.; Cooper, J.; Zhang, G.; Boskovic, D.S.; Kwon, S.R.; Nick, K.E.; Perry, C.C. Role of TiO_2 Anatase Surface Morphology on Organophosphorus Interfacial Chemistry. *J. Phys. Chem. C* **2018**, *122*, 29237–29248. [CrossRef]
66. Bader, R.F.W. A Bond Path: A Universal Indicator of Bonded Interactions. *J. Phys. Chem. A* **1998**, *102*, 7314–7323. [CrossRef]
67. Bader, R.F.W.; Essén, H. The characterization of atomic interactions. *J. Chem. Phys.* **1984**, *80*, 1943–1960. [CrossRef]
68. Cremer, D.; Kraka, E. A Description of the Chemical Bond in Terms of Local Properties of Electron Density and Energy. *Croat. Chem. Acta* **1984**, *57*, 1259–1281.
69. Espinosa, E.; Molins, E.; Lecomte, C. Hydrogen bond strengths revealed by topological analyses of experimentally observed electron densities. *Chem. Phys. Lett.* **1998**, *285*, 170–173. [CrossRef]
70. Espinosa, E.; Alkorta, I.; Rozas, I.; Elguero, J.; Molins, E. About the evaluation of the local kinetic, potential and total energy densities in closed-shell interactions. *Chem. Phys. Lett.* **2001**, *336*, 457–461. [CrossRef]
71. Borissova, A.O.; Antipin, M.Y.; Karapetyan, H.A.; Petrosyan, A.M.; Lyssenko, K.A. Cooperativity effects of H-bonding and charge transfer in an L-nitroarginine crystal with Z′ > 1. *Mendeleev Commun.* **2010**, *20*, 260–262. [CrossRef]
72. Baryshnikov, G.V.; Minaev, B.F.; Minaeva, V.A.; Nenajdenko, V.G. Single crystal architecture and absorption spectra of octathio[8]circulene and *sym*-tetraselenatetrathio[8]circulene: QTAIM and TD-DFT approach. *J. Mol. Model.* **2013**, *19*, 4511–4519. [CrossRef] [PubMed]
73. Baryshnikov, G.V.; Minaev, B.F.; Korop, A.A.; Minaeva, V.A.; Gusev, A.N. Structure of zinc complexes with 3-(pyridin-2-yl)-5-(arylideneiminophenyl)-1HH-1,2,4-triazoles in different tautomeric forms: DFT and QTAIM study. *Russ. J. Inorg. Chem.* **2013**, *58*, 928–934. [CrossRef]
74. Shahangi, F.; Chermahini, A.N.; Farrokhpour, H.; Teimouri, A. Selective complexation of alkaline earth metal ions with nanotubular cyclopeptides: DFT theoretical study. *RSC Adv.* **2014**, *5*, 2305–2317. [CrossRef]
75. Puntus, L.N.; Lyssenko, K.A.; Antipin, M.Y.; Bünzli, J.C.G. Role of Inner- and Outer-Sphere Bonding in the Sensitization of EuIII-Luminescence Deciphered by Combined Analysis of Experimental Electron Density Distribution Function and Photophysical Data. *Inorg. Chem.* **2008**, *47*, 11095–11107. [CrossRef]